

See discussions, stats, and author profiles for this publication at: <https://www.researchgate.net/publication/231648608>

# Synthesis of Magnetite/Graphene Oxide Composite and Application for Cobalt(II) Removal

ARTICLE in THE JOURNAL OF PHYSICAL CHEMISTRY C · DECEMBER 2011

Impact Factor: 4.77 · DOI: 10.1021/jp208575m

---

CITATIONS

120

READS

392

## 5 AUTHORS, INCLUDING:



Changlun Chen

Chinese Academy of Sciences

98 PUBLICATIONS 6,454 CITATIONS

[SEE PROFILE](#)



Xi-Lin Wu

Zhejiang Normal University

23 PUBLICATIONS 773 CITATIONS

[SEE PROFILE](#)



Xiangke Wang

Chinese Academy of Sciences

307 PUBLICATIONS 13,375 CITATIONS

[SEE PROFILE](#)

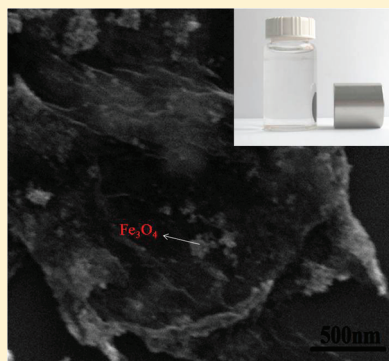
# Synthesis of Magnetite/Graphene Oxide Composite and Application for Cobalt(II) Removal

Mancheng Liu, Changlun Chen,\* Jun Hu, Xilin Wu, and Xiangke Wang\*

Key Laboratory of Novel Thin Film Solar Cells, Institute of Plasma Physics, Chinese Academy of Sciences, P.O. Box 1126, Hefei 230031, People's Republic of China

Supporting Information

**ABSTRACT:** A magnetite/graphene oxide (M/GO) composite was synthesized via a chemical reaction with a magnetite particle size of 10–15 nm and was developed for the removal of heavy metal ions from aqueous solutions. The composite was characterized by scanning electron microscopy, transmission electron microscopy, X-ray diffraction, and X-ray photoelectron spectroscopy. The sorption of Co(II) on the M/GO composite was carried out under various conditions, that is, contact time, sorbent content, pH, ionic strength, foreign ions, and temperature. The sorption isotherms of Co(II) on the M/GO composite could be described well by the Langmuir model. The thermodynamic parameters ( $\Delta H^0$ ,  $\Delta S^0$ , and  $\Delta G^0$ ) calculated from the temperature-dependent isotherms indicated that the sorption reaction of Co(II) on the M/GO composite was an endothermic and spontaneous process. M/GO can be separated and recovered by magnetic separation. Results show that the magnetic M/GO composite is a promising sorbent material for the preconcentration and separation of heavy metal ions from aqueous solutions.



## 1. INTRODUCTION

Co(II) can cause several health troubles, such as low blood pressure, lung irritations, paralysis, diarrhea, and bone defects. Therefore, the removal of Co(II) from the aqueous solution is crucial for the environmental protection. In the last decades, several methods, such as precipitation, coprecipitation, oxidation, ion-exchange, reverse osmosis, membrane electrolysis, and sorption, were employed to remove Co(II) ions from large volumes of aqueous solutions.<sup>1–3</sup> Although all these methods afford moderate to efficient removal of heavy metal ions, sorption technology is one of the most effective choices for the removal of heavy metal ions from aqueous solutions due to its simplicity of design, convenience, low cost, high sorption efficiency, and wide adaptability. Various materials, such as clay minerals, oxides, zeolites, and carbon materials, have been used as adsorbents. However, there are still some problems that limit their practical application, such as adsorption capacity is not high enough, the adsorbent is difficult to separate, and so on. As a result, searching for new adsorbents to solve these problems is of significant importance.

Graphene oxide (GO) is a lamellar flexible material with a wide range of functional groups, such as epoxy (C—O—C), hydroxyl (OH), and carboxyl (COOH) groups, on both basal planes and edges.<sup>4</sup> Therefore, it can be easily exfoliated and functionalized to form homogeneous suspensions in both water and organic solvents,<sup>5</sup> providing more possibility for synthesis of graphene-based materials.<sup>6–8</sup> The existence of oxygen functional groups and aromatic sp<sup>2</sup> domains allow GO to participate in a wide range of bonding interactions. Many graphene-based

multifunctional hybrid materials have been synthesized by using graphene oxide. In our earlier report,<sup>9</sup> sulfonated graphene was used to remove persistent aromatic pollutants.

Recently, magnetic graphene oxide and magnetic graphene composites have been fabricated and have shown good properties for drug delivery,<sup>10</sup> energy storage,<sup>11,12</sup> and water treatment.<sup>13</sup> The magnetic property, 2D structure, and existence of active sites make the magnetic graphene oxide a good substrate for synthesis of magnetic graphene-based composites.

In this work, the magnetic magnetite/graphene oxide (M/GO) composite was first synthesized and characterized by scanning electron microscopy (SEM), transmission electron microscopy (TEM), X-ray diffraction (XRD), and X-ray photoelectron spectroscopy (XPS), and then the application of the magnetic composite for the removal of Co(II) from aqueous solutions was investigated by batch experiments.

## 2. EXPERIMENTAL SECTION

**2.1. Materials.** Graphite powder (70  $\mu$ m, Qingdao Graphite Company), 98% H<sub>2</sub>SO<sub>4</sub>, ammonia solution, KMnO<sub>4</sub>, FeCl<sub>3</sub>·6 H<sub>2</sub>O, 30% H<sub>2</sub>O<sub>2</sub>, glycol, and all other chemicals were reagent grade and purchased from Sinopharm Chemical Reagent Co. Ltd.. Milli-Q (Millipore, Billerica, MA, USA) water was used in all experiments.

**Received:** September 6, 2011

**Revised:** October 31, 2011

**Published:** November 28, 2011

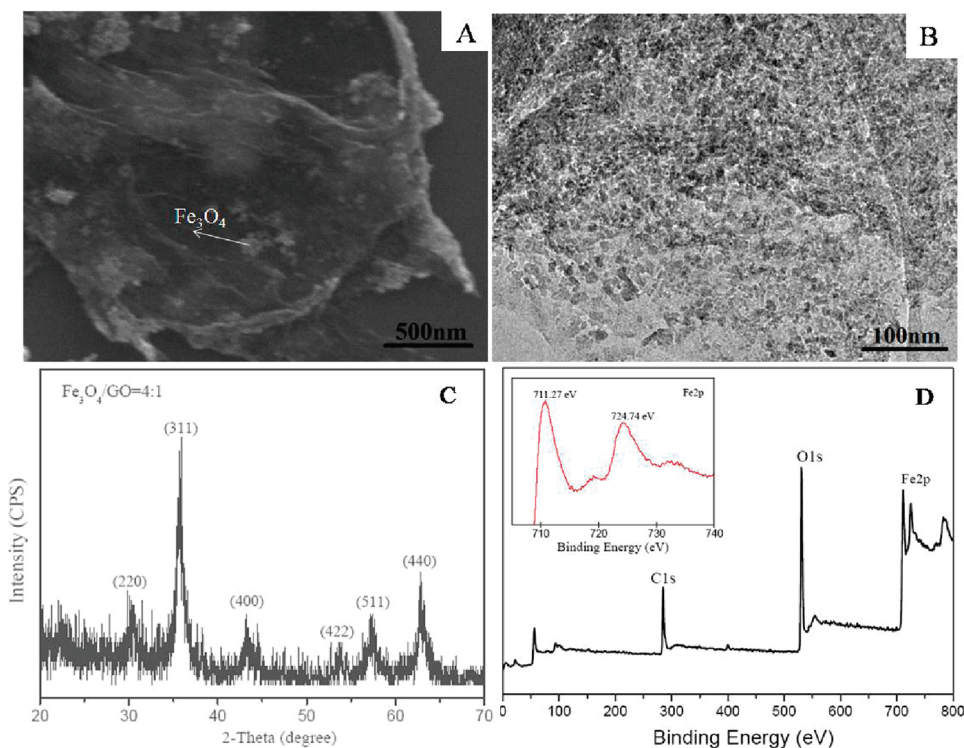


**Figure 1.** (A) SEM and (B) TEM images, (C) XRD pattern, and (D) XPS spectrum of the M/GO composite (the inset illustrates the high-solution spectrum of the Fe 2p peak of the composite).

**2.2. Preparation of Graphene Oxide.** Graphene oxide was synthesized from natural graphite by a modified Hummers and Offeman's method,<sup>14,15</sup> where 98% H<sub>2</sub>SO<sub>4</sub> was added to graphite powder and NaNO<sub>3</sub>; then KMnO<sub>4</sub> was gradually added while stirring. The rate of addition was carefully controlled to keep the reaction temperature below 20 °C. Subsequently, the reaction mixture was diluted with Milli-Q water in an ice bath where the temperature was rapidly increased to 98 °C. The suspension was stirred at 98 °C for 1 day. H<sub>2</sub>O<sub>2</sub> (30%) was then added to the mixture. The resulting suspension was heated using a microwave oven (Haier, 2450 MHz, 700 W) for 5 min. Finally, the solid GO was obtained after the black deposit was filtered, washed several times with Milli-Q water and alcohol, and dried at 100 °C for 12 h in a vacuum oven.

**2.3. Preparation of M/GO Composite.** The M/GO composite was synthesized by coprecipitation of FeCl<sub>3</sub>·6H<sub>2</sub>O and FeCl<sub>2</sub>·4H<sub>2</sub>O, in the presence of GO. The mixed water solution of FeCl<sub>3</sub> and FeCl<sub>2</sub> was added slowly to the GO solution, and ammonia solution was added quickly to precipitate Fe<sup>2+</sup>/Fe<sup>3+</sup> ions for synthesis of magnetite (Fe<sub>3</sub>O<sub>4</sub>) particles. The temperature was raised to 85 °C, and a 30% ammonia solution was added to adjust the pH to 10. After being rapidly stirred for 45 min, the solution was cooled to room temperature. The dark black colored solution was then filtered and washed with Milli-Q water/ethanol and dried in vacuum at 70 °C. The M/GO composite was then prepared. The weight ratio of magnetite to GO was 4:1.

**2.4. Characterization.** The SEM image was obtained with a JEOL JSM-6330F. The TEM image was performed on a JEOL-2010 microscope. The XRD pattern was recorded on a (Philips X'Pert Pro Super X-ray) diffractometer with a Cu K $\alpha$  source ( $\lambda = 1.54178 \text{ \AA}$ ). The XPS measurements were performed in a VG

Scientific ESCALAB Mark II spectrometer equipped with two ultra-high-vacuum (UHV) chambers. Magnetic measurement was performed in a MPMS-XL SQUID magnetometer.

**2.5. Batch Sorption Experiments.** All the experiments were performed using a batch technique in the polyethylene centrifuge tubes under ambient conditions. The stock solutions of the M/GO composite, NaCl, and Co(II) were added to achieve the desired background electrolyte concentration of different components. The pH was adjusted to the desired values by adding negligible amounts of 0.1 or 0.01 M HCl or NaOH. The test tubes were shaken for 24 h to achieve equilibrium. The samples were then separated by a magnetic process using a permanent magnet. The concentration of Co(II) was measured using an atomic absorption spectrophotometer. The amount of Co(II) adsorbed on the M/GO composite was calculated from the difference between the initial concentration and the equilibrium one. The sorption percentage and the distribution coefficient ( $K_d$ ) are calculated from the following equations

$$K_d = \frac{C_0 - C_e}{C_e} \times \frac{V}{m} \quad (1)$$

$$\text{Sorption \%} = \frac{C_0 - C_e}{C_0} \times 100\% \quad (2)$$

where  $C_0$  is the initial concentration ( $\text{mg L}^{-1}$ ),  $C_e$  is the equilibrium concentration ( $\text{mg L}^{-1}$ ),  $m$  (g) is the mass of the M/GO composite, and  $V$  (mL) is the volume of the suspension. All the experimental data were the averages of duplicate or triplicate determinations. The relative errors of the data were about 5%.

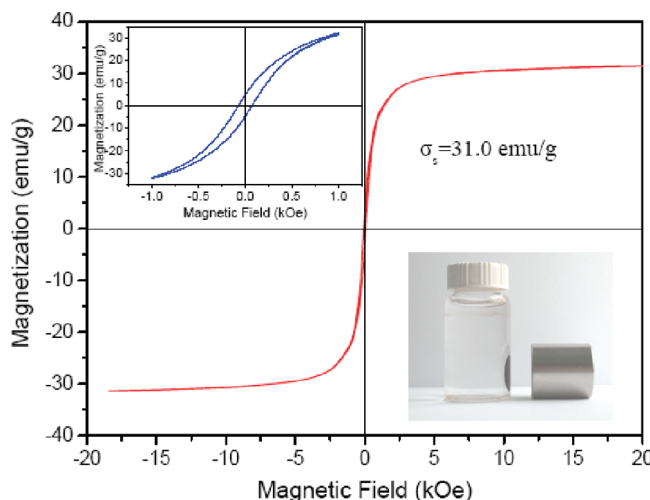


**Figure 2.** Magnetization curve at room temperature of the M/GO composite, indicating that M/GO has a high magnetism.

### 3. RESULTS AND DISCUSSION

**3.1. Characterization of the Magnetic M/GO Composite.** The typical SEM and TEM images of the magnetic M/GO composite are shown in Figure 1. From Figure 1A, it can be seen clearly that GO sheets are the matrix of  $\text{Fe}_3\text{O}_4$  nanoparticles and some wrinkles are observed on the surface of the M/GO composite, which may be important for preventing aggregation of GO and loading magnetic nanoparticles. As shown in Figure 1B, the graphene oxide sheets are disorderly distributed between the closely packed  $\text{Fe}_3\text{O}_4$  nanoparticles. Closer examination reveals that the average size of the  $\text{Fe}_3\text{O}_4$  nanoparticles is about 10–15 nm.

Figure 1C shows the XRD pattern of the M/GO structure. The intense diffraction peaks indexed to (2 2 0), (3 1 1), (4 0 0), (4 2 2), (5 1 1), and (4 4 0) planes appearing at  $2\theta = 30.15, 36.27, 43.32, 53.89, 57.13$ , and  $62.29^\circ$ , respectively, are consistent with the standard XRD data for the cubic phase  $\text{Fe}_3\text{O}_4$  with a face-centered cubic (fcc) structure. The broad diffraction peaks are indications of the nanoparticles with very small sizes.

The chemical state of elements in the M/GO composite was further investigated by X-ray photoelectron spectroscopy (XPS). The wide scan XPS spectrum (Figure 1D) of the M/GO composite shows photoelectron lines at a binding energy of about 285, 530, and 711 eV attributed to C 1s, O 1s, and Fe 2p, respectively. In the spectrum of Fe 2p (the inset of Figure 1D), the peaks of Fe 2p<sub>3/2</sub> and Fe 2p<sub>1/2</sub> are located at 711.27 and 724.74 eV, not at 710.34 and 724.02 eV, which are for  $\text{Fe}_2\text{O}_3$ .<sup>16</sup> The result is in accordance with the reported data of Fe 2p<sub>3/2</sub> and Fe 2p<sub>1/2</sub>, which is indicative of the formation of the  $\text{Fe}_3\text{O}_4$  phase in the composite. XPS can also be used to identify groups attached to the surfaces of the M/GO composite. The obtained data were calibrated by using the adventitious carbon at a binding energy of 284.5 eV. The deconvoluted C 1s XPS spectra of the M/GO composite show three peaks at 284.6, 286.2, and 287.9 eV, and they correspond to C–C, C–O, and C=O bonds, respectively (see Figure S11 in the Supporting Information).

The magnetization property of the M/GO composite was investigated at room temperature by measuring the magnetization curve (Figure 2). The saturation magnetization ( $M_s$ ) of the M/GO composite is 31 emu g<sup>-1</sup> (magnetic field  $\pm 20$  kOe),

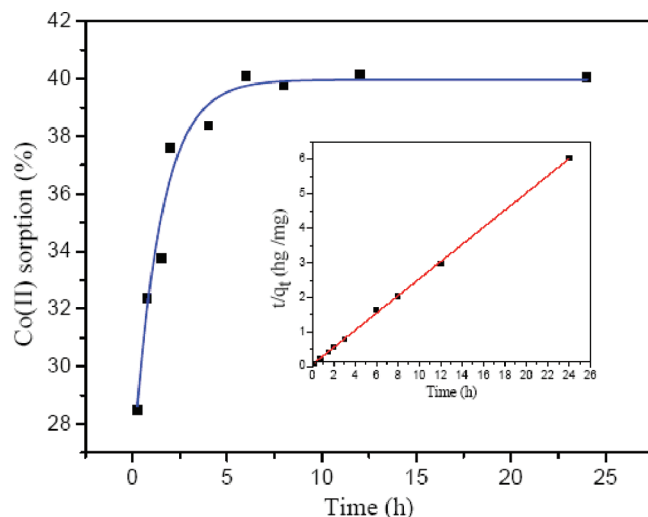


**Figure 3.** Time-dependent Co(II) sorption onto the M/GO composite, at  $\text{pH} = 6.8 \pm 0.1$ ,  $T = 303.15 \text{ K}$ ,  $I = 0.01 \text{ M NaCl}$ ,  $C_{\text{Co(II)} \text{ initial}} = 10.0 \text{ mg L}^{-1}$ ,  $m/V = 0.4 \text{ g L}^{-1}$ .

indicating that the M/GO composite has a high magnetism. The inset of Figure 2 shows that the particles of the M/GO composite are attracted quickly toward a magnet. Co(II) is first adsorbed onto the M/GO composite to achieve equilibrium, and then the M/GO composite-bound Co(II) is sequestered from the aqueous solution by a magnet at the moment and the clear solution can be easily removed by pipet or decanted off. The result of this simple magnetic separation experiment confirms that the M/GO composite is magnetic and can be used as a magnetic adsorbent to remove pollutants from large volumes of aqueous solutions in real work.

**3.2. Time-Dependent Sorption.** The sorption of Co(II) from aqueous solution to the M/GO composite as a function of contact time is shown in Figure 3. The sorption of Co(II) on the M/GO composite is rapid over the first 5 h of contact time and then remains constant with increasing contact time. In the following experiments, 24 h was selected to ascertain the sorption equilibrium of Co(II) to the M/GO composite. The fast sorption velocity indicates that strong chemisorption or strong surface complexation contributes to the sorption of Co(II) on the M/GO composite. The results that the sorption is quick to achieve equilibrium are important for the application of the M/GO composite to remove metal ions from aqueous solutions in real work.

To analyze the sorption rate of Co(II) on the M/GO composite, a pseudo-second-order rate equation was used to simulate the kinetic sorption<sup>17,18</sup>

$$\frac{t}{q_t} = \frac{1}{2K'q_e^2} + \frac{t}{q_e} \quad (3)$$

where  $K'$  (g mg<sup>-1</sup> h<sup>-1</sup>) is the pseudo-second-order rate constant of sorption,  $q_t$  (mg g<sup>-1</sup> of dry weight) is the amount of Co(II) adsorbed on the surface of the M/GO composite at time  $t$  (h), and  $q_e$  (mg g<sup>-1</sup> of dry weight) is the equilibrium sorption capacity. A linear plot feature of  $t/q_t$  vs  $t$  is achieved and inserted in Figure 3. The  $K'$  value calculated from the slope and intercept is  $0.557 \text{ g mg}^{-1} \text{ h}^{-1}$ . The correlation coefficient ( $R = 0.9995$ ) for the linear plot is very close to 1, which suggests that kinetic

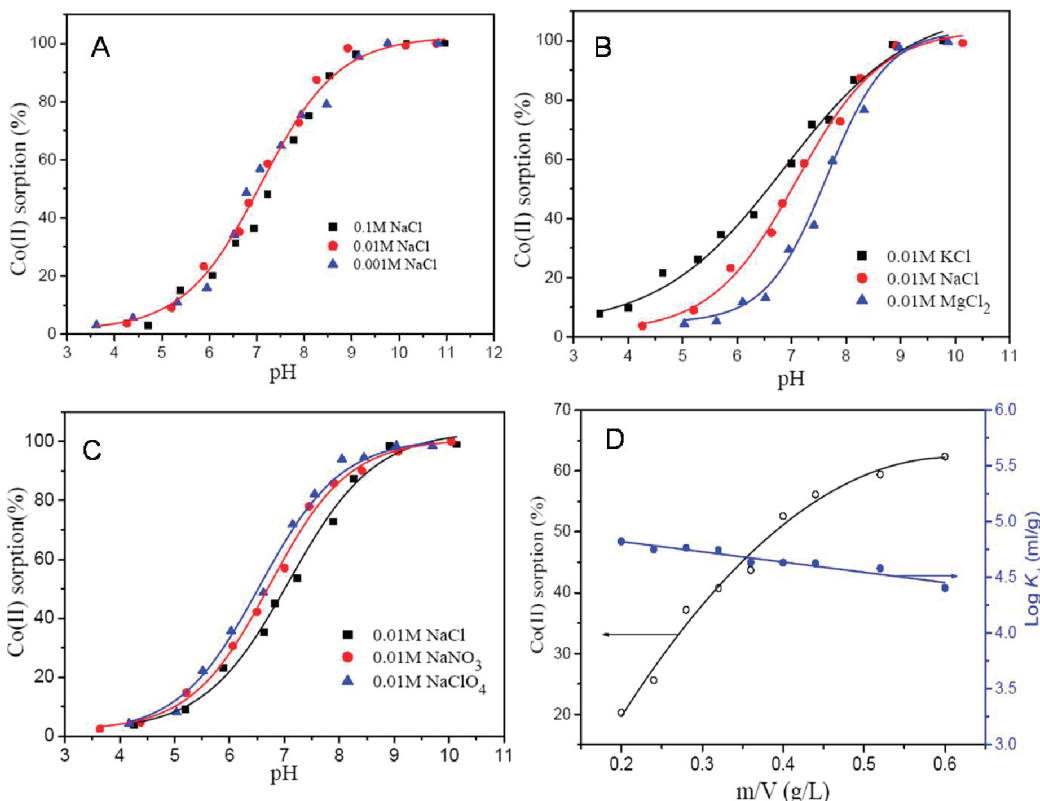


**Figure 4.** Effect of ionic strength (A), foreign cations (B), foreign anions (C), and sorbent content (D) on Co(II) sorption onto the M/GO composite, at pH = 6.8 ± 0.1, T = 303.15 K, I = 0.01 M NaCl, C<sub>Co(II)</sub> initial = 10.0 mg L<sup>-1</sup>.

sorption is very well described by a pseudo-second-order rate equation.

**3.3. Effect of Environmental Conditions.** In general, the removal of metal ions from an aqueous solution is dependent on the solution pH, ionic strength, adsorbent content, and other parameters. Therefore, it is important to study whether the variance of these parameters affects the removal of metal ions by M/GO or not.

The sorption values of Co(II) on the M/GO composite as a function of pH in 0.1, 0.01, and 0.001 M NaCl solutions are shown in Figure 4A. As can be seen, the pH of the aqueous solution plays an important role in the sorption of Co(II) on the M/GO composite. With the initial concentration ( $C_0$ ) of 10 mg L<sup>-1</sup>, the sorption of Co(II) on the M/GO composite increases slowly at pHs ranging from 3 to 6, then increases abruptly at pH 6–8.5, and at last retains the high sorption with increasing pH at pH > 8.5. About 95% of Co(II) is adsorbed on the M/GO composite at pH > 8.5. The strong pH-dependent sorption suggests that Co(II) sorption on the M/GO composite is attributed to inner-sphere surface complexation rather than ion exchange or outer-sphere surface complexation.

The relative species of cobalt are present in aqueous solutions in the forms of Co<sup>2+</sup>, Co(OH)<sup>+</sup>, Co(OH)<sub>2</sub>, and Co(OH)<sub>3</sub><sup>-</sup> at different pH values. The relative species distribution of Co(II) calculated from the hydrolysis constants ( $\log K_1 = -9.6$ ,  $\log K_2 = -9.2$ , and  $\log K_3 = -12.7$ )<sup>19</sup> are shown in Figure SI2 (Supporting Information). At pH < 8.5, the predominant species are Co<sup>2+</sup> and Co(OH)<sup>+</sup>. Because of the protonation reaction (i.e.,  $\equiv\text{SOH} + \text{H}^+ \leftrightarrow \equiv\text{SOH}_2^+$ ) on the surfaces of the M/GO composite, the concentration of protonated sites ( $\equiv\text{SOH}_2^+$ )

decreases with increasing pH. Thereby, the sorption of Co<sup>2+</sup> and Co(OH)<sup>+</sup> on the M/GO composite is unfavorable as a result of the Coulombic repulsion at a pH range of 3–6. However, at high pH values, the concentration of deprotonated sites ( $\equiv\text{SO}^-$ ) increases with increasing pH because of the surface deprotonation reaction (i.e.,  $\equiv\text{SOH} \leftrightarrow \equiv\text{SO}^- + \text{H}^+$ ). The deprotonated sites ( $\equiv\text{SO}^-$ ) are more available to retain the metal ions, and surface complexation between Co<sup>2+</sup>, Co(OH)<sup>+</sup>, and the M/GO composite is facilitated, thus resulting in a sharp increase of Co(II) sorption at pH 6–8.5. Co(OH)<sub>2</sub> precipitation begins to form at pH > 8.5.

The effect of ionic strength on the sorption of Co(II) to the M/GO composite was studied by carrying out a series of experiments at varying concentrations of NaCl solutions. As illustrated in Figure 4A, the effect of ionic strength in a wide pH range is fairly negligible. The ionic strength affects the thickness and interface potential of the double layer (the background solution and the surface of the M/GO composite), influencing the binding of the adsorbing species. The background electrolyte ions are placed in the same plane as the outer-sphere complexes; thus, outer-sphere surface complexes are expected to be more susceptible to ionic-strength variations than inner-sphere surface complexes. Consequently, the sorption of Co(II) on the M/GO composite may suggest the formation of inner-sphere complexes on the surfaces of the M/GO composite. The ionic strength-independent and pH-dependent Co(II) sorption on the M/GO composite indicate that the sorption mechanism of Co(II) is inner-sphere surface complexation at low pH values, whereas the removal of Co(II) is accomplished by simultaneous precipitation and inner-sphere surface complexation at high pH values.

To investigate the influence of foreign ions on Co(II) sorption, the sorption of Co(II) on the M/GO composite was studied as a function of pH values in 0.01 mol L<sup>-1</sup> NaCl, MgCl<sub>2</sub>, KCl, NaNO<sub>3</sub>, and NaClO<sub>4</sub>. From Figure 4B, the sorption of Co(II) on the M/GO composite is strongly affected by the foreign cations at pH < 9. The sorption of Co(II) on the M/GO composite under the same pH values is in the following sequence: K<sup>+</sup> > Na<sup>+</sup> > Mg<sup>2+</sup>, indicating that cations can alter the surface property of the M/GO composite and thus can affect the sorption of Co(II) on the M/GO composite. Yang et al.<sup>20</sup> investigated the effect of foreign cations on Ni(II) sorption to oxidized MWCNTs and also found a similar result. The sorption of Co(II) on the M/GO composite can be considered as a competition of Co(II) with foreign cations (K<sup>+</sup>, Na<sup>+</sup>, and Mg<sup>2+</sup>) at the M/GO composite surfaces. The higher valence ion is much easier to be adsorbed on the adsorbent surface; thereby, the influence of Mg<sup>2+</sup> on Co(II) sorption is stronger than that of Na<sup>+</sup> and K<sup>+</sup>. The radius of Na<sup>+</sup> is smaller than that of K<sup>+</sup>; therefore, Na<sup>+</sup> has the higher affinity to the surface of the M/GO composite and the higher tendency for counterion complexation with the surface groups of the M/GO composite, which reduces ion interaction sites on the surface of the M/GO composite with Co(II). The result leads to that the influence sequence of foreign alkali metal ions on sorption of Co(II) to the M/GO composite is in the range of Na<sup>+</sup> > K<sup>+</sup>.

In general, the influence of alkali metal and alkaline earth cations on the sorption of bivalent Co(II) should be weak. However, in this work, the concentration of the foreign cations ( $1.00 \times 10^{-2}$  mol L<sup>-1</sup>) is much higher than that of Co(II) ( $1.7 \times 10^{-4}$  mol L<sup>-1</sup>). At pH < 9, the sorption of Co(II) on the M/GO composite can be attributed to the exchange of Co(II) with alkali metal or alkaline earth cations. Thereby, it is reasonable that the coexisting foreign cations can affect the sorption of Co(II) on the M/GO composite. One can also see that no drastic difference of Co(II) sorption to the M/GO composites in the foreign cation solutions is observed at pH > 9, which may be due to surface precipitates at high pH values.

From Figure 4C, the sorption of Co(II) on the M/GO composite is the highest in 0.01 mol L<sup>-1</sup> NaClO<sub>4</sub> solution and is the lowest in 0.01 mol L<sup>-1</sup> NaCl solution at pH < 8.5. This phenomenon may be attributed to the following: (1) compared with NO<sub>3</sub><sup>-</sup> and ClO<sub>4</sub><sup>-</sup>, Cl<sup>-</sup> is easier to form idiopathic sorption on the solid surface, which changes the surface state of the M/GO composite and decreases the availability of binding sites; (2) Cl<sup>-</sup> and NO<sub>3</sub><sup>-</sup> can form soluble complexes with Co(II) (e.g., CoCl<sup>+</sup> and CoNO<sub>3</sub><sup>+</sup>), whereas ClO<sub>4</sub><sup>-</sup> does not form complexes with Co(II), and Co(II) has a higher affinity with Cl<sup>-</sup> than NO<sub>3</sub><sup>-</sup> and ClO<sub>4</sub><sup>-</sup>; and (3) the inorganic acid radical radius order is Cl<sup>-</sup> < NO<sub>3</sub><sup>-</sup> < ClO<sub>4</sub><sup>-</sup>, and the smaller radius inorganic acid radicals take up more ionic exchange sites, which leads to the decrease of Co(II) sorption on the M/GO composite.

The effect of solid content on the sorption of Co(II) on the M/GO composite is shown in Figure 4D. The sorption of Co(II) increases obviously with increasing solid content. This trend is expected because the functional sites that participate in the sorption of Co(II) increase with increasing solid content, and more sites of sorption form on the M/GO composite. The distribution coefficient ( $K_d$ ) plotted in Figure 4D decreases a little with increasing solid content. The decrease of  $K_d$  values with increasing solid content may be attributed to the competition among the colloids of the M/GO composite. Such competition reduces the effective sites of functional groups at the surface of the M/GO composite and results in the decreasing of the

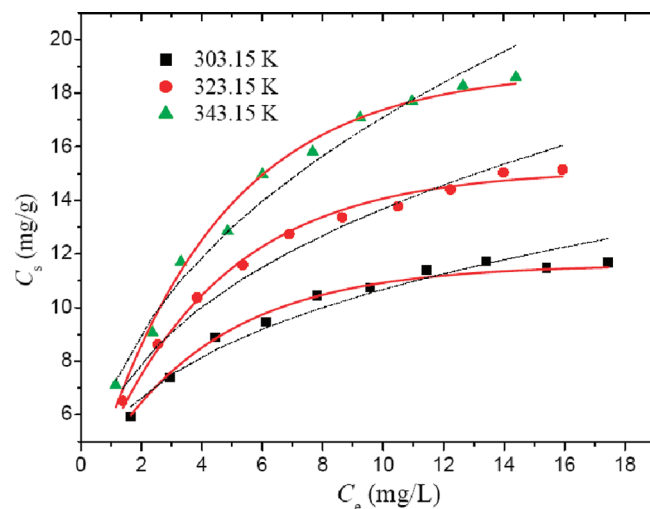


**Figure 5.** Sorption isotherms of Co(II) onto the M/GO composite at three different temperatures, at pH = 6.8 ± 0.1,  $I = 0.01$  M NaCl,  $m/V = 0.4$  g L<sup>-1</sup>. The scattered points represent experiment data. The solid lines represent the Langmuir model. The dashed lines represent the Freundlich model.

sorption and complexation ability of the M/GO composite with increasing solid content.

**3.4. Sorption Isotherms.** The sorption isotherms obtained at 303.15, 323.15, and 343.15 K are shown in Figure 5. With the increasing of Co(II) concentration, the sorption first increases rapidly and then increases slowly. Sorption isotherms become higher in the order of 303.15, 323.15, and 343.15 K; that is, the process of sorption is favored at high temperatures. To gain a better understanding of sorption mechanisms and to quantify the sorption data, the Langmuir and Freundlich models were used to simulate the experimental data.

The Langmuir isotherm model was used to describe the monolayer sorption process. Its form can be expressed by the following equation:<sup>21</sup>

$$C_s = \frac{bC_{s\ max}C_e}{1 + bC_e} \quad (4)$$

Equation 4 can be expressed in the line form

$$\frac{C_e}{C_s} = \frac{1}{bC_{s\ max}} + \frac{C_e}{C_{s\ max}} \quad (5)$$

where  $C_{s\ max}$  (mg g<sup>-1</sup>), the maximum sorption capacity, is the amount of Co(II) at complete monolayer coverage, and  $b$  (L mg<sup>-1</sup>) is the constant that relates to the heat of sorption.

The Freundlich isotherm model allows for several kinds of sorption sites on the solid and represents properly the sorption data at low and intermediate concentrations on heterogeneous surfaces. The model can be represented by the following equation:<sup>22</sup>

$$C_s = K_F C_e^n \quad (6)$$

Equation 6 can be expressed in line form

$$\log C_s = \log K_F + n \log C_e \quad (7)$$

where  $K_F$  (mol<sup>1-n</sup> L<sup>n</sup> g<sup>-1</sup>) represents the sorption capacity when the metal ion equilibrium concentration is equal to 1 and  $n$

**Table 1.** Parameters for the Langmuir and Freundlich Isotherm Models at Different Temperatures

T (K)	Langmuir			Freundlich		
	$C_{s\ max}$ (mg g <sup>-1</sup> )	b (L mg <sup>-1</sup> )	R <sup>2</sup>	K <sub>F</sub> (mol <sup>1-n</sup> ·L <sup>n</sup> g <sup>-1</sup> )	n	R <sup>2</sup>
303.15	12.98	0.498	0.995	5.44	0.293	0.960
323.15	17.58	0.380	0.999	6.26	0.340	0.971
343.15	22.70	0.315	0.994	6.86	0.397	0.978

represents the degree of dependence of sorption with equilibrium concentration.

The sorption isotherms of Co(II) on the M/GO composite are regressively analyzed with the Langmuir and Freundlich models, which are shown in Figure SI3 (Supporting Information). The related parameters of the two models are listed in Table 1. From the correlation coefficients ( $R^2$ ) and fitting curves shown in Figure 5, one can see that the Langmuir model fits the experimental data better than the Freundlich model. The fact that the sorption data of Co(II) is in accordance with the Langmuir isotherm indicates that monolayer coverage of the sorbent particles is the main sorption mechanism. The values of  $C_{s\ max}$  calculated from the Langmuir model for Co(II) sorption on the M/GO composite are the lowest at  $T = 303.15$  K and the highest at  $T = 343.15$  K, which indicates that the sorption is enhanced with increasing temperature.

The thermodynamic parameters ( $\Delta G^0$ ,  $\Delta S^0$ , and  $\Delta H^0$ ) used to define whether the sorption of Co(II) on the M/GO composite is endothermic or exothermic and spontaneous can be calculated from the temperature-dependent sorption. The free energy change ( $\Delta G^0$ ) is derived from the relationship

$$\Delta G^0 = -RT \ln K^0 \quad (8)$$

where  $K^0$  is the sorption equilibrium constant. Values of  $\ln K^0$  are obtained by plotting  $\ln K_d$  versus  $C_e$  (Figure SI4, Supporting Information) and extrapolating  $C_e$  to zero. Constants of the linear fit of  $\ln K_d$  versus  $C_e$  for sorption of Co(II) on the M/GO composite are listed in Table SI1 (Supporting Information). Its intercept with the vertical axis gives the value of  $\ln K^0$ . The standard entropy change ( $\Delta S^0$ ) is calculated using the equation

$$\Delta S^0 = - \left( \frac{\partial \Delta G^0}{\partial T} \right)_P \quad (9)$$

The average standard enthalpy change ( $\Delta H^0$ ) is then calculated from the relationship

$$\Delta H^0 = \Delta G^0 + T\Delta S^0 \quad (10)$$

where  $R$  (8.314 J mol<sup>-1</sup> K<sup>-1</sup>) is the ideal gas constant and  $T$  (K) is the temperature in kelvin. The thermodynamic data calculated by eqs 8–10 are listed in Table 2. The positive value of the standard enthalpy change indicates that the sorption is endothermic, and it is consistent with the increasing sorption as the temperature increases. One interpretation for the positive enthalpy may be that Co(II) is dissolved well in water and the hydration sheath of Co(II) has to be destroyed before its sorption on the M/GO composite. This dehydration process needs energy, and high temperature is beneficial for sorption.<sup>23</sup> This energy exceeds the exothermicity of cations to attach to the solid surface. The assumption indicates that the endothermicity

**Table 2.** Values of Thermodynamic Parameters for Co(II) Sorption on the M/GO Composite

T (K)	$\Delta G^0$ (kJ mol <sup>-1</sup> )	$\Delta S^0$ (J mol <sup>-1</sup> K <sup>-1</sup> )	$\Delta H^0$ (kJ mol <sup>-1</sup> )
303.15	-19.94	100.00	10.38
323.15	-21.92	100.00	10.39
343.15	-23.94	100.00	10.38

of the desolvation process is higher than the enthalpy of sorption to a considerable extent. The Gibbs free energy change ( $\Delta G^0$ ) is negative, as expected for a spontaneous process under the conditions applied. That the value of  $\Delta G^0$  becomes more negative with the increase of temperature indicates more efficient sorption at higher temperature. At high temperature, cations are readily desolvated, and hence their sorption becomes more favorable.<sup>24</sup> The positive value of the entropy change ( $\Delta S^0$ ) hints at the affinity of the M/GO composite toward Co(II) ions in aqueous solutions and may suggest some structural changes on the composite.<sup>25–27</sup> Above all, it can be concluded that the sorption of Co(II) on the M/GO composite is an endothermic and spontaneous process from the thermodynamic parameters of the sorption isotherms.

Figure SI5 (Supporting Information) illustrates the adsorption isotherms of Co(II) on M/GO and Fe<sub>3</sub>O<sub>4</sub>. The adsorption isotherms of Co(II) on two different adsorbents were simulated by the Langmuir model. The maximum adsorption capacities of Co(II) are 12.98 mg g<sup>-1</sup> for the M/GO composite and 6.2 mg g<sup>-1</sup> for Fe<sub>3</sub>O<sub>4</sub>. The results indicate that the adsorption capacity of Co(II) on the M/GO composite is much higher than that of Co(II) on Fe<sub>3</sub>O<sub>4</sub>, which is attributed to the high adsorption ability of Co(II) on graphene oxide. Table SI2 (Supporting Information) shows a comparison of the Langmuir adsorption capacity of the M/GO composite with that of other common adsorbents documented in the literature, indicating the excellent adsorption abilities of the M/GO composite toward Co(II).

#### 4. CONCLUSIONS

The analysis results of SEM, TEM, XRD, and XPS indicated that the M/GO composite was synthesized. The sorption of Co(II) on M/GO followed the pseudo-second-order model very well. The ionic strength-independent and pH-dependent Co(II) sorption on M/GO indicated that the sorption mechanism of Co(II) was inner-sphere surface complexation at low pH values, whereas the removal of Co(II) was accomplished by simultaneous precipitation and inner-sphere surface complexation at high pH values. The sorption of Co(II) on M/GO was influenced by foreign ions. The thermodynamic parameters calculated from the temperature-dependent isotherms indicated that the sorption reaction of Co(II) on the M/GO composite was an endothermic and spontaneous process. M/GO-bound Co(II) can be quickly separated and recovered from a solution by easy magnetic separation. The magnetic composite of the M/GO composite is a very suitable material for metal ion pollution cleanup in the natural environment. With the development of the preparation technology of graphene, the cost of graphene will be reduced and graphene and graphene composites will be used for real work in the near future. The content in this paper is relevant and important for the application of a magnetic separation method and graphene oxide in environmental pollution cleanup.

## ■ ASSOCIATED CONTENT

**S Supporting Information.** The deconvoluted C 1s XPS spectra of the M/GO composite; linear regression of Langmuir and Freundlich isotherms of Co(II) sorption; linear plots of  $\ln K_d$  versus  $C_e$ ; and comparison of Co(II) adsorption on M/GO, Fe<sub>3</sub>O<sub>4</sub>, and other adsorbents. This material is available free of charge via the Internet at <http://pubs.acs.org>.

## ■ AUTHOR INFORMATION

### Corresponding Author

\*Fax: +86-551-5591310. Phone: +86-551-5592788. E-mail: clchen@ipp.ac.cn (C.C.), xkwang@ipp.ac.cn (X.W.).

## ■ ACKNOWLEDGMENT

Financial support from the 973 project of MOST (2011CB933700) and the National Natural Science Foundation of China (21071147, 21107115, 21077107, 91126020, 20971126) is acknowledged.

## ■ REFERENCES

- (1) El-Dessouky, S. I.; El-Sofany, E. A.; Daoud, J. A. *J. Hazard. Mater.* **2007**, *143*, 17–23.
- (2) Xu, D.; Shao, D. D.; Chen, C. L.; Ren, A. P.; Wang, X. K. *Radiochim. Acta* **2006**, *94*, 97–102.
- (3) Yavuz, Ö.; Altunkaynak, Y.; Güzel, F. *Water Res.* **2003**, *37*, 948–952.
- (4) Lerf, A.; He, H. Y.; Forster, M.; Klinowski, J. *J. Phys. Chem. B* **1998**, *102*, 4477–4482.
- (5) He, H. K.; Gao, C. *Chem. Mater.* **2010**, *22*, 5054–5064.
- (6) Watcharotone, S.; Dikin, D. A.; Stankovich, S.; Piner, R.; Jung, I.; Dommett, G. H. B.; Evmenenko, G.; Wu, S.-E.; Chen, S.-F.; Liu, C.-P.; Nguyen, S. T.; Ruoff, R. S. *Nano Lett.* **2007**, *7*, 1888–1892.
- (7) Yang, X. Y.; Wang, Y. S.; Huang, X.; Ma, Y. F.; Huang, Y.; Yang, R. C.; Duan, H. Q.; Chen, Y. S. *J. Mater. Chem.* **2011**, *21*, 3448–3454.
- (8) Lambert, T. N.; Chavez, C. A.; Hernandez-Sanchez, B.; Lu, P.; Bell, N. S.; Ambrosini, A.; Friedman, T.; Boyle, T. J.; Wheeler, D. R.; Huber, D. L. *J. Phys. Chem. C* **2009**, *113*, 19812–19823.
- (9) Zhao, G. X.; Jiang, L.; He, Y. D.; Li, J. X.; Dong, H. L.; Wang, X. K.; Hu, W. P. *Adv. Mater.* **2011**, *23*, 3959–3963.
- (10) Chen, C.; Cai, W.; Long, M.; Zhou, B.; Wu, Y.; Wu, D.; Feng, Y. *ACS Nano* **2010**, *4*, 6425–6432.
- (11) Zhou, G. M.; Wang, D. W.; Li, F.; Zhang, L. L.; Li, N. Z.; Wu, S.; Wen, L.; Lu, G. Q.; Cheng, H. M. *Chem. Mater.* **2010**, *22*, 5306–5313.
- (12) Zhang, M.; Lei, D. N.; Yin, X. M.; Chen, L. B.; Li, Q. H.; Wang, Y. G.; Wang, T. H. *J. Mater. Chem.* **2010**, *20*, 5538–5543.
- (13) Koo, H. Y.; Lee, H. J.; Go, H. A.; Lee, Y. B.; Bae, T. S.; Kim, J. K.; Choi, W. S. *Chem.—Eur. J.* **2011**, *17*, 1214–1219.
- (14) Hummers, W. S.; Offeman, R. E. *J. Am. Chem. Soc.* **1958**, *80*, 1339–1341.
- (15) Jahan, M.; Bao, Q. L.; Yang, J. X.; Loh, K. P. *J. Am. Chem. Soc.* **2010**, *132*, 14487–14495.
- (16) Lu, J.; Jiao, X.; Chen, D.; Li, W. *J. Phys. Chem. C* **2009**, *113*, 4012–4017.
- (17) Tan, X. L.; Chen, C. L.; Yu, S. M.; Wang, X. K. *Appl. Geochem.* **2008**, *23*, 2767–2777.
- (18) Ho, Y. S. *J. Hazard. Mater.* **2006**, *B136*, 681–689.
- (19) Yuzer, H.; Kara, M.; Sabah, E.; Celik, M. S. *J. Hazard. Mater.* **2008**, *151*, 33–37.
- (20) Yang, S. T.; Li, J. X.; Shao, D. D.; Hu, J.; Wang, X. K. *J. Hazard. Mater.* **2009**, *166*, 109–116.
- (21) Langmuir, I. *J. Am. Chem. Soc.* **1918**, *40*, 1361–1403.
- (22) Chen, C. L.; Hu, J.; Shao, D. D.; Li, J. X.; Wang, X. K. *J. Hazard. Mater.* **2009**, *164*, 923–928.
- (23) Sheng, G. D.; Li, J. X.; Shao, D. D.; Hu, J.; Chen, C. L.; Chen, Y. X.; Wang, X. K. *J. Hazard. Mater.* **2010**, *178*, 333–340.
- (24) Tahir, S. S.; Rauf, N. *J. Chem. Thermodyn.* **2003**, *35*, 2003–2009.
- (25) Genc-Fuhrman, H.; Tjell, J. C.; McConchie, D. *Environ. Sci. Technol.* **2004**, *38*, 2428–2434.
- (26) Zhao, G. X.; Zhang, H. X.; Fan, Q. H.; Ren, X. M.; Li, J. X.; Chen, Y. X.; Wang, X. K. *J. Hazard. Mater.* **2010**, *173*, 661–668.
- (27) Chen, C. L.; Wang, X. K. *Ind. Eng. Chem. Res.* **2006**, *45*, 9144–9149.